Photosynthetic Hydrogen Production by a Hybrid Complex of Photosystem I and [NiFe]-Hydrogenase

Henning Krassen,[†,⊥] Alexander Schwarze,[‡,⊥] Bärbel Friedrich,[‡] Kenichi Ataka,[†,§] Oliver Lenz,[‡] and Joachim Heberle[†,§,*]

[†]Department of Chemistry, Bielefeld University, D-33615 Bielefeld, Germany, [‡]Institute of Biology, Humboldt-Universität zu Berlin, D-10115 Berlin, Germany, [§]Department of Physics, Freie Universität, D-14195 Berlin, Germany, and [⊥]These authors contributed equally to this work

ABSTRACT Nature provides key components for generating fuels from renewable resources in the form of enzymatic nanomachines which catalyze crucial steps in biological energy conversion, for example, the photosynthetic apparatus, which transforms solar power into chemical energy, and hydrogenases, capable of generating molecular hydrogen. As sunlight is usually used to synthesize carbohydrates, direct generation of hydrogen from light represents an exception in nature. On the molecular level, the crucial step for conversion of solar energy into H_2 lies in the efficient electronic coupling of photosystem I and hydrogenase. Here we show the stepwise assembly of a hybrid complex consisting of photosystem I and hydrogenase on a solid gold surface. This device gave rise to light-induced H_2 evolution. Hydrogen production is possible at far higher potential and thus lower energy compared to those of previously described (bio)nanoelectronic devices that did not employ the photosynthesis apparatus. The successful demonstration of efficient solar-to-hydrogen conversion may serve as a blueprint for the establishment of this system in a living organism with the paramount advantage of self-replication.

KEYWORDS: nanobiotechnology · bionanotechnology · hydrogenase · photosystem · biohydrogen production

Fuels from renewable sources, such as molecular hydrogen, are necessary to satisfy the growing global energy demand in the future without creating severe environmental problems.[1] A promising approach is to use nature's catalytic converter of solar power into chemical energy—the photosynthesis apparatus[2]—to convert solar energy into biomass at a rate of 90 TJ s^{-1}.[3] Using light as the driving force, photosystem II (PS II) splits water into molecular oxygen, protons, and electrons. The latter are transferred to the chlorophyll *a* dimer (P700) residing in photosystem I (PS I). Upon light absorption, P700 is excited, yielding electrons at a potential of −1.32 V (*vs* NHE).[4] Finally, electrons are conducted through the internal electron transfer chain to the iron−sulfur clusters F_A and F_B, which are located at the acceptor site of PS I at a potential of approximately −0.45 V.[5]

Both photosystems have previously been used in electrochemical setups to convert light energy into electrical energy. This includes solid-state devices and protein monolayers immobilized on gold nanoparticles or nanoporous gold electrodes.[6−10] In a recent study, platinum nanoparticles have been tethered to the F_B cluster of PS I *via* a dithiol molecular wire. Upon illumination, this semiartificial system generated up to 70 mol H_2 mol^{-1} PS I min^{-1}.[11] However, a catalyst more efficient than the noble metal platinum is provided by nature. Hydrogenases are metalloenzymes that either oxidize or evolve H_2 with an overpotential close (or equal) to 0 V.[12,13] These abilities make them attractive for application as catalysts in electrocatalytic devices.[14−17]

Connections between photosynthesis and H_2 production already exist in nature. Both cyanobacteria and green algae accumulate reserve compounds such as glycogen or starch from light and CO_2 during the daytime. At nighttime, when photosynthesis is shut off, these reserve compounds provide the energy to run the cellular metabolism. The transition from aerobic to anaerobic conditions is often accompanied by the generation of excess reductant, which is finally turned into hydrogen by hydrogenase (for recent reviews see refs 18−20). Hence, the processes of photosynthesis and H_2 evolution are coupled only indirectly and time-delayed. Moreover, hydrogen conversion by cyanobacterial and algal hydrogenases is sensitive to dioxygen. This intrinsic restriction makes it difficult to generate hydrogen at the same time as the O_2-evolving PS II works at a normal level. However, a significant increase of net H_2 production was achieved by limiting PS II activity by sulfur limitation of green algae. This strategy also depends on a

*Address correspondence to joachim.heberle@uni-bielefeld.de.

Received for review July 6, 2009 and accepted November 13, 2009.

Published online November 30, 2009.
10.1021/nn900748j

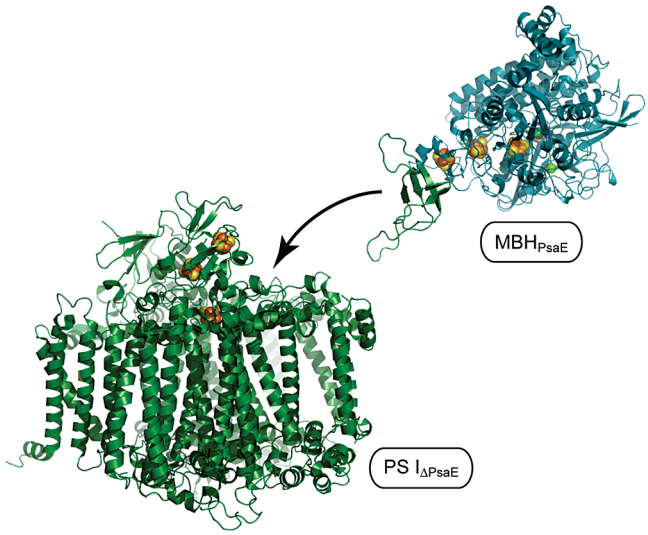

Figure 1. Coupling concept of PS I$_{\Delta PsaE}$ and MBH$_{PsaE}$. The peripheral *PsaE* subunit of photosystem I (PS I) from *Synechocystis* sp. PCC 6803 was genetically fused to the membrane-bound [NiFe]-hydrogenase (MBH) of *Ralstonia eutropha* H16. The MBH$_{PsaE}$ fusion protein binds specifically and spontaneously to the *PsaE* deletion mutant of PS I (PS I$_{\Delta PsaE}$). The structures are derived from the following PDB entries: 1JB0 for PS I from *Thermosynechococcus elongates*, 2FRV for the periplasmic [NiFe]-hydrogenase from *Desulfovibrio gigas*, which is homologous to the MBH.[2,25]

two-stage cultivation process, nevertheless, it possesses the highest light-to-H_2 conversion rate to date.[21]

In order to overcome the above-mentioned constraints, we aim at the direct coupling of photosynthesis and H_2 production. This strategy implicitly requires an O_2-tolerant hydrogenase. Therefore, we employed the oxygen-tolerant membrane-bound hydrogenase (MBH) from *Ralstonia eutropha* H16 for which it has been shown that H_2 oxidation as well as H_2 evolution proceeds in the presence of O_2.[16,22] In order to stably connect the MBH to PS I, the extrinsic *PsaE* subunit, which is located at the acceptor site of PS I, was fused to the electron-transferring subunit of the membrane-bound [NiFe]-hydrogenase by genetic engineering. The resulting MBH$_{PsaE}$ protein was purified and incubated with isolated PS I from *Synechocystis* sp. PCC 6803 lacking the *PsaE* subunit (PS I$_{\Delta PsaE}$). PS I$_{\Delta PsaE}$ and MBH$_{PsaE}$ were assembled on a gold surface yielding a PS I−hydrogenase hybrid complex (Figure 1). Electrons provided by the gold electrode were transferred to PS I with the aid of the soluble electron carrier *N*-methylphenazonium methyl sulfate (PMS).[23] Upon excitation of P700, the electrons were efficiently channelled to the hydrogenase, leading to H_2 evolution through proton reduction (Figure 2). A similar protein complex was recently investigated in solution, but hydrogen production rates have not been quantified on the basis of the amount of hydrogenase attached to PS I.[24]

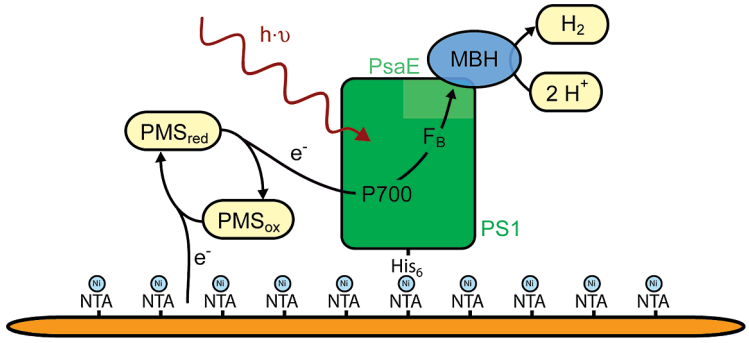

Figure 2. Schematic view of the nanodevice used in this study. Electrons provided by the gold electrode reduce the oxidized form of *N*-methylphenazonium methyl sulfate (PMS). PMS transfers an electron to the chlorophyll *a* dimer P700 in PS I, which is promoted to a higher energy level upon illumination. The electrons are then transferred *via* the F_B cluster at the acceptor site to the distal iron−sulfur cluster of the hydrogenase (MBH) and further to the active site where protons are reduced to molecular hydrogen.

Here we immobilized the hybrid complex onto the solid support of a gold electrode. It is shown by surface-enhanced infrared spectroscopy (SEIRAS) and electrochemistry that both proteins specifically assemble on the surface and electrons are transferred between both proteins, respectively. We applied surface plasmon resonance and gas chromatography in order to determine the hydrogen evolution activity quantified per molecule and surface area. These data offer this nanoelectronic device as a platform technology that allows comparison of different coupling methods and catalytic building blocks (*e.g.*, different hydrogenases).

Directed Assembly of the PS I−Hydrogenase Hybrid Complex on a Gold Electrode. By genetic engineering, a decahistidine tag was attached to the periplasmic side of the membrane-integral *PsaF* subunit of wild-type PS I (PS I$_{wt}$) and to PS I, which had been deleted for the *PsaE* subunit (PS I$_{\Delta PsaE}$). This strategy allowed site-oriented attachment of both PS I variants to the electrode surface *via* histidine/Ni-NTA interaction. The orientation was chosen to expose the *PsaE* binding site to the bulk solution. The fabrication of the Ni-NTA-terminated gold surface was performed essentially as described.[26]

In order to test whether MBH$_{PsaE}$ interacts with PS I, monolayers of PS I$_{\Delta PsaE}$ and PS I$_{wt}$ were established on the gold surface by injecting solutions of purified photosystem preparations into the bulk electrolyte at a final concentration of 0.5 μM. In a second step, the PS I monolayers were incubated with a 1.4 μM solution of MBH$_{PsaE}$. The absorption changes, caused by binding of hydrogenase to the PS I monolayers, were recorded *in situ* by surface-enhanced infrared spectroscopy (Figure 3). Binding of MBH$_{PsaE}$ to PS I$_{\Delta PsaE}$ was saturated after 2 h (Supporting Information Figure S1).

After incubation with MBH$_{PsaE}$, the surface was thoroughly rinsed with buffer to remove weakly associated protein. The SEIRA spectra of the immobilized fusion protein MBH$_{PsaE}$ showed two prominent bands at 1660 and 1549 cm^{-1}, which were assigned to the amide I (predominantly C═O stretching vibration of the peptide bound) and amide II (C═N stretch coupled to

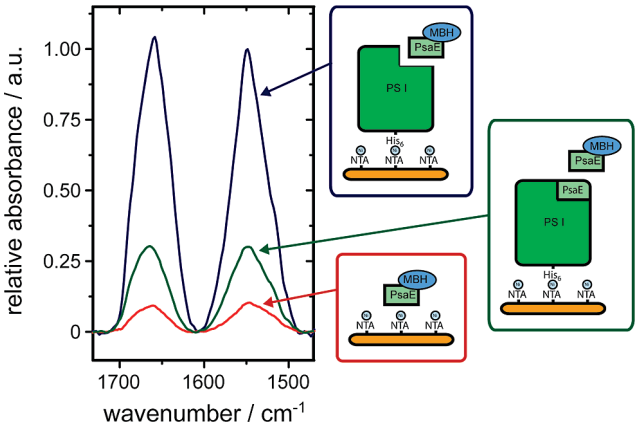

Figure 3. SEIRA spectra demonstrating the specific binding of MBH_{PsaE} to PS $I_{\Delta PsaE}$. The MBH_{PsaE} fusion protein was added to monolayers of PS $I_{\Delta PsaE}$ (blue trace), PS I_{wt} (green trace), and bare Ni-NTA (red trace). The background spectra derived from the PS I monolayers were subtracted from the sample spectra, which were taken after surface saturation with MBH_{PsaE} (2 h, Supporting Information Figure S1). The spectra were normalized to the surface enhancement factor of the respective gold surface (Supporting Information Figure S2) and to 1 for the amide II intensity of the blue curve.

the N−H bend) vibrations, respectively.[27] The frequency of the absorption maximum of the amide I band at 1660 cm^{-1} is indicative for a predominant α-helical structure of MBH.

In order to compare the relative amount of adsorbed MBH_{PsaE}, the integrated areas of the amide II bands were compared. Maximal binding was observed for MBH_{PsaE} immobilized to the PS $I_{\Delta PsaE}$ monolayer. The respective integrated area was set to 100% (Figure 3, blue trace). This result is consistent with the previous observation that isolated *PsaE* spontaneously binds to *PsaE*-free PS I to re-establish the fully functional photosynthetic complex.[28,29] It is important to note that specific assembly (*i.e.*, binding of the *PsaE* moiety of MBH_{PsaE} to its native binding site in PS $I_{\Delta PsaE}$) and all possible unspecific and unproductive interactions contributed to the intensity of the amide II band. The MBH_{PsaE} fusion protein, which was not equipped with a His-tag, interacted only weakly with the Ni-NTA monolayer *via* unspecific electrostatic interactions (Figure 3, red trace). The MBH_{PsaE} also binds to wild-type PS I as determined by SEIRAS (Figure 3, green trace). However, the affinity is only 37% as shown by comparison to the deletion mutant PS $I_{\Delta PsaE}$ (blue spectrum). Consequently, we conclude that the difference in binding efficiency (approximately 2/3 of the maximum binding) was due to specific interaction between MBH and PS I, mediated by the *PsaE* subunit of PS I, which was genetically swapped to MBH.

Immobilization of MBH_{PsaE} onto the PS $I_{\Delta PsaE}$ monolayer was quantified by surface plasmon resonance (SPR, Supporting Information Figure S3). The SPR response increased by 2,850 RU during the binding process, which corresponds to a protein coverage of 2.85 ng MBH_{PsaE} mm^{-2} (or 2.5×10^{-12} mol MBH_{PsaE} cm^{-2}).[30,31] Taking into account that about two-thirds of MBH_{PsaE} was bound specifically to PS $I_{\Delta PsaE}$, we calculated the amount of hydrogenase specifically immobilized on PS $I_{\Delta PsaE}$ to be 1.9 ng MBH_{PsaE} mm^{-2} (or 1.6×10^{-12} mol cm^{-2}).

Photocurrent of the PS I−Hydrogenase Hybrid Complex. *PsaE* and MBH were genetically fused to bring the electron-conducting terminal iron−sulfur cluster of the MBH into close contact to the acceptor site of PS I represented by the F_B cluster. Taking the structures of *Desulfovibrio gigas* hydrogenase (PDB-ID: 2FRV) and PS I from *Thermosynechococcus elongatus* (PDB-ID: 1JB0) as structural models for the MBH and PS I, we estimated the distance between F_B and the distal iron−sulfur cluster of the MBH to be 14−25 Å depending on the mutual orientation of the hydrogenase relative to PS I. To verify light-induced electron transfer (photocurrent) from PS I to MBH experimentally, we applied amperometry. The anticipated electron flow is depicted in Figure 2. At a potential of −90 mV (*vs* NHE), the soluble electron carrier PMS, whose midpoint potential is +85 mV (Supporting Information), was reduced by the electrode and served as electron donor for the reaction center P700 in PS I. Upon red-light illumination, PS I promoted the electron transfer to the MBH active site where protons from the bulk were reduced to H_2. PMS, oxidized by PS I, diffused back to the electrode where it was re-reduced.

The PS $I_{\Delta PsaE}$ monolayer exhibited a photocurrent density of 55 nA cm^{-2} (Figure 4, dotted trace), which on one hand can be explained by the reduction of residual oxygen at the PS I acceptor site. In fact, it has been shown previously that *PsaE* prevents the formation of reduced oxygen species.[32] On the other hand, however, it is rather likely that PMS and protons (see

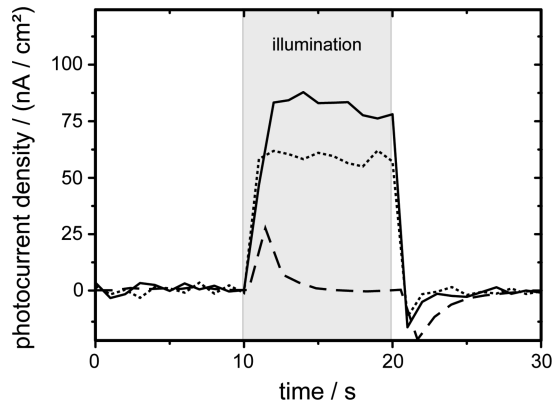

Figure 4. Photocurrent of the PS I−hydrogenase hybrid complex. Monolayers of the PS I−MBH hybrid complex (solid trace) and sole PS $I_{\Delta PsaE}$ (dotted trace) as well as the bare gold electrode (dashed trace) were illuminated for 10 s with red light (λ_{max} = 702 nm, fwhm = 16 nm, gray area). The experiments were done in a closed reaction chamber filled with argon-purged buffer. The current density was corrected for the background current observed without red light illumination (see Materials and Methods).

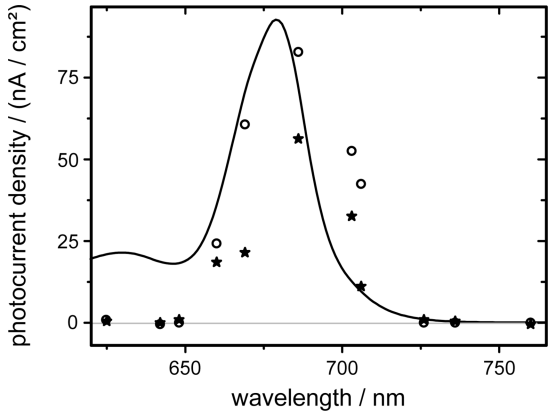

Figure 5. Action spectra of PS I-derived photocurrents. The photocurrent at different wavelengths is shown for monolayers of the PS I−hydrogenase hybrid complex (open circles) and PS $I_{\Delta PsaE}$ (asterisks). The photocurrents are normalized to the relative surface coverage. The absorption spectrum of a bulk solution of PS $I_{\Delta PsaE}$ is shown for comparison (black trace).

below) are directly reduced at the acceptor site, resulting in the PS I photocurrent. This process might even be alleviated by the fact that the lack of *PsaE* improves unspecific accessibility to the acceptor site.[32]

Formation of the functional PS I−MBH complex led to an significant increase of the photocurrent density from 55 to approximately 85 nA cm^{-2} (Figure 4, solid trace), suggesting that binding of MBH provided a suitable electron acceptor close to the acceptor site of PS I. The significant rise in current implies that at least 30% of the photocurrent density can be assigned to H_2 formation. The bare gold surface, illuminated under the same conditions (Figure 4, dashed trace), exhibited only capacitive currents, visible as sharp peaks upon switching light on and off. However, no photocurrent was observed in this control.

As a control that the photocurrent was dependent on the presence of functional PS I, we measured the wavelength dependence of the photocurrent (action spectrum) of the hybrid complex (Figure 5, open circles) and PS $I_{\Delta PsaE}$ (asterisks). Maximum photocurrent was observed at a wavelength of 685 nm for both constructs. The match of the individual data taken at different wavelengths was not perfect but tallies with the absorption spectrum of the PS I core complex (Figure 5, black trace). The core antenna chlorophylls absorb in a broad band with a maximum at 680 nm and provide energy for P700.[33] The action spectrum verified that the measured photocurrent was derived from PS I and also showed that the presence of the hydrogenase did not influence the photoreaction.

Hydrogen Evolution by the PS I−Hydrogenase Hybrid Complex. The electrochemical experiments described above provided only indirect evidence that the photocurrent by the PS I−hydrogenase hybrid might be used for H_2 production. Therefore, a monolayer of the hybrid complex was assembled on the gold surface in a gastight measuring cell. After 30 min of illumination, accumulated H_2 was quantified by gas chromatography. From these measurements, the rate of H_2 production per time and electrode area was calculated. Upon illumination, the immobilized PS I−MBH hybrid complex generated molecular hydrogen at a rate of 120 ± 30 pmol H_2 s^{-1} cm^{-2} at an electrode potential of −90 mV (to re-reduce PMS). The photocurrent of the monolayer decreased by about 50% during 30 min of illumination (data not shown). As the photocurrent is a prerequisite for hydrogen production, we infer that the initial rate of H_2 production is higher.

TABLE 1. Hydrogen Evolution Rates

surface structure	illumination	H_2 production rate/(pmol H_2 s^{-1} cm^{-2})
PS I−MBH	yes	120 ± 30
PS I−MBH	no	<20
PS $I_{\Delta PsaE}$	yes	31 ± 12
MBH	yes	<20
bare gold	yes	<20

It was surprising to note that H_2 was produced from a monolayer of PS $I_{\Delta PsaE}$ at a rate of 31 ± 12 pmol H_2 s^{-1} cm^{-2} even in the absence of hydrogenase. This observation of a weak but significant H_2 production rate (~1/4 of the PS I−MBH hybrid complex) suggests that electrons provided at the acceptor site of PS I ($F_{A/B}$) can be directly used to reduce protons to molecular hydrogen. The midpoint potentials of the terminal clusters F_A/F_B range between −0.45[5] and −0.59 V.[34] It is noteworthy that H_2 production by low-potential iron−sulfur clusters has not been described yet in the literature, and a potential of −0.6 V is insufficient for H_2 production at bare gold electrodes at pH of 7.5.[17] However, it is well-known that the overpotential for proton reduction on metal electrodes can be lowered by the addition of small organic molecules, like 4,4′-bipyridine, methyl viologen, or pyridine.[35−38] From these observations, we conclude that H_2 production may proceed at low rates in the protein scaffold of low-potential iron−sulfur clusters.

The observation of light-induced hydrogen production was verified by the following control experiments (Table 1). First, H_2 production by the PS I−MBH hybrid complex was strictly dependent on light and, hence, did not proceed in the dark. Second, the bare gold surface as well as His-tagged MBH directly immobilized onto the Ni-NTA-terminated gold surface did not exhibit hydrogen production rates higher than the threshold level of 20 pmol H_2 s^{-1} cm^{-2} (at −90 mV and under illumination). These experiments confirm that light-dependent activation of low-potential electrons by PS I is necessary for H_2 evolution activity.

On the basis of the hydrogen production rate of the PS I−hydrogenase hybrid complex (120 × 10^{-12} mol H_2 s^{-1} cm^{-2}) as determined by gas chromatography and the amount of MBH_{PsaE} specifically bound to PS $I_{\Delta PsaE}$ (1.6 × 10^{-12} mol MBH_{PsaE} cm^{-2}) as determined

by SEIRAS and SPR, the specific surface activity is calculated to be 4500 ± 1125 mol H_2 min^{-1} mol^{-1} hybrid complex (at pH 7.5, 20 °C, −90 mV). In comparison, MBH directly immobilized on a pyrolytic graphite edge electrode (in the absence of PS I) exhibited a turnover rate of 4200 mol H_2 min^{-1} mol^{-1}, which was estimated to be the lower limit.[16] This rate which was measured at a potential of −450 mV, pH 5.5, 40 °C, and during continuous removal of the produced hydrogen, is in close agreement with the light-dependent H_2 evolution rate of the PS I−MBH complex (4500 mol H_2 min^{-1} mol^{-1}, *vide supra*). Very importantly, the light-induced promotion of electrons through PS I made it possible to increase the electrode potential from −450 to −90 mV (to lower energy), to increase the pH to 7.5, and to decrease the temperature by 20 °C without decreasing the hydrogen evolution rate.

CONCLUSIONS

In this article, we demonstrated the specific and productive connection of a hydrogenase to PS I. Both proteins were assembled on a gold surface in a well-defined manner. Upon light illumination, the PS I−MBH hybrid complex produced molecular hydrogen at a rate of 4500 ± 1125 mol H_2 min^{-1} mol^{-1} hybrid complex (at pH 7.5, 20 °C, −90 mV). Light energy is used to allow hydrogen production at more positive potential (and thus lower energy) than on platinum electrodes which are commercially used for proton reduction. Furthermore, electronic connection between PS I and hydrogenase is completely independent of chemically synthesized linker molecules, such as 1,6-hexanedithiol.[11] This system is, therefore, superior to previously described (bio)nanoelectronic devices for hydrogen production and provides a blueprint for biologically inspired H_2 production systems.[16,17] Owing to the exceptional O_2 tolerance of the hydrogenase used in the experiments, the hydrogenase−PS I hybrid complex can be synthesized *in vivo*, yielding a cellular system that efficiently produces H_2 directly from sunlight and water.

MATERIAL AND METHODS

Purification of Proteins. By standard genetic techniques, the C-terminal "anchor" sequence, encoded by the 3′-end of the MBH small subunit gene *hoxK*, was replaced by an Arg-Ser linker followed by a Strep-tagII peptide. In the next step, a sequence encoding *PsaE* from *Synechocystis* sp. PCC 6803 equipped with a N-terminal Gly-Gly linker was inserted between *hoxK* and the Strep-tagII sequence. The resulting MBH_{PsaE} fusion protein was purified from *Ralstonia eutropha* by Strep-Tactin affinity chromatography.

Purification of MBH wild-type protein was facilitated by fusing a hexahistidine-coding sequence to the 3′-end of the MBH small subunit *hoxK*.[39] Fast and easy purification of PS I derivatives from *Synechocystis* was afforded by fusing a decahistidine-encoding sequence genetically to the 5′-end of the *psaF* gene that codes for a membrane-integral subunit of PS I. The His_{10}-*psaF* allele was transformed into the *Synechocystis* PS I_{wt} and PS $I_{\Delta PsaE}$ strains and established in the respective genomes. The resulting PS I and PS $I_{\Delta PsaE}$ proteins were purified from *Synechocystis* sp. PCC 6803 by immobilized metal-affinity chromatography and hydrophobic interaction chromatography. The detailed construction and purification procedures for the protein components employed in this study will be described elsewhere.

Surface-Enhanced Infrared Adsorption Spectroscopy (SEIRAS) and Spectroelectrochemistry. A gold film was chemically deposited on the reflecting side of a triangular silicon prism.[40−42] A glass cell was mounted on top of the silicon prism. The gold film was exposed to the electrolyte and used as working electrode. The electrochemical cell was equipped with a Ag/AgCl/3 M KCl reference electrode and a platinum mesh counter electrode. All electrodes were connected to a potentiostat (Autolab PGSTAT 12, Eco Chemie B.V., Utrecht, The Netherlands). All potentials are quoted *versus* the normal hydrogen electrode (NHE) (0.21 V *vs* Ag/AgCl/3 M KCl)). The IR beam from the FT-IR spectrometer (Vertex 70, Bruker Optics, Ettlingen, Germany) was coupled into the single reflection silicon prism at an incident angle of 60°. The intensity of the reflected beam was measured by an MCT detector; 910 scans were averaged for each sample and background spectrum.

Surface Modification for SEIRAS Experiments. To assemble a Ni-NTA-terminated monolayer, the gold surface was successively exposed to solutions of 2.5 mM dithiobis(succinimidyl propionate) (DTSP, Sigma), 150 mM N_α,N_α-bis(carboxymethyl)-L-lysine (Sigma) and 50 mM $NiSO_4$.[26] The Ni-NTA-terminated surface was incubated with a solution of 0.5 μM wild-type PS I or PS I lacking the *PsaE* subunit (PS $I_{\Delta PsaE}$) dissolved in 20 mM Hepes buffer (pH 7.5) containing 0.03% β-dodecylmaltosid (β-DDM), 10 mM $MgCl_2$, and 10 mM $CaCl_2$. In the last step, the surface was incubated in a 1.4 μM solution of the fusion protein of the PS I subunit *PsaE* and the membrane-bound hydrogenase (MBH_{PsaE}) (in the same buffer as PS I, but containing only 1 mM $MgCl_2$ and 1 mM $CaCl_2$). All surface modification steps using PS I or PS $I_{\Delta PsaE}$ were performed at 20 °C in the dark.

Surface Plasmon Resonance. Surface plasmon resonance (SPR) experiments were performed on a Biacore 3000 (GE Healthcare, Uppsala, Sweden) with a constant flow rate of 5 μL min^{-1}. Fresh Au sensorchips were used to provide an untreated gold surface for each experiment. The untreated gold surface was rinsed with 300 μL of aqueous 1 mM 3-mercaptopropionic acid solution to form a carboxy-terminated self-assembled monolayer (SAM). Fifteen microliters of an aqueous solution of the coupling reagent *N*-(3-dimethylaminopropyl)-*N*′-ethylcarbodiimide (containing hydrochloric acid, pH 4) was injected to activate the carboxylic acid groups on the surface. Then, 375 μL of N_α,N_β-bis(carboxymethyl)-L-lysine hydrate (ANTA) in 0.2 M solution of potassium carbonate was injected and a carboxamide linkage was formed between ANTA and the carboxylic acid groups on the surface. Rinsing with 150 μL nickel sulfate is the last step to form a Ni-NTA-covered surface. Consecutive rinsing with 650 μL of a 300 μg mL^{-1} solution of the *PsaE*-free PS I (in 20 mM HEPES (pH 7.5) containing 0.03% β-dodecylmaltosid (β-DDM), 10 mM $MgCl_2$, and 10 mM $CaCl_2$) and 325 μL of a 170 μg mL^{-1} solution of the fusion protein of *PsaE* and the membrane-bound hydrogenase (MBH_{PsaE}) (in the same buffer as PS I, but containing only 1 mM $MgCl_2$ and 1 mM $CaCl_2$) yielded the surface-bound hybrid complex. A wedge-shaped, near-infrared beam is focused on the glass−gold interface of the sensorchip, and the reflected light is monitored by a two-dimensional diode array. The intensity of the reflected light is significantly reduced at the resonance angle. This angle depends on the refractive index, which is associated with the sample.

Photocurrent Measurement. A monolayer of the hybrid complex of photosystem I and membrane-bound hydrogenase (PS I−MBH) was formed on the Ni-NTA-modified surface. The gold electrode had a geometrical surface of 1.45 cm^2 and a surface roughness of 2.5.[42] *N*-Methylphenazonium methyl sulfate (PMS, 75 μM) was used as the soluble electron carrier between the

gold surface and PS I. The system was equilibrated at pH 7.5 and under potential control until the current flow through the solution was constant and most of the PMS was reduced. The photocurrent was measured during illumination by a cold light source (KL 1500 electronic, Schott, Mainz, Germany) with suitable interference filters. All experiments were performed under an argon atmosphere.

***In Vitro* Hydrogen Production.** After the surface modification was completed, the system was purged with argon for at least 20 min to remove atmospheric oxygen and traces of hydrogen. No traces of hydrogen could be detected in the argon. Then, the chamber was sealed gastight and illuminated by red light for 30 min at a potential of −90 mV. A sample of 1 mL of the gas phase was taken from the measurement cell and injected into a gas chromatograph (3000A Micro GC, Agilent Technologies, Santa Clara, CA) to determine the amount of evolved hydrogen. The gas chromatograph was calibrated by injection of defined amounts of hydrogen, which were in the same order of magnitude as the hydrogen produced by the protein monolayers. *In vitro* hydrogen production was also determined for immobilized His-tagged MBH on the gold surface by the same procedure.

Note added in proof: In a recent article, Iwuchukwu and coworkers describe the hydrogen production by platinized PSI nanoparticles with a maximum yield of 5.5 μmol H_2 h^{-1} per mg of chlorophyll (Iwuchukwu, I. J.; Vaughn, M.; Myers, N.; O'Neill, H.; Frymier, P.; Bruce, B. D. Self-Organized Photosynthetic Nanoparticle for Cell-Free Hydrogen Production. *Nat. Nanotechnol.* **2009** DOI: 10.1038/NNANO.2009.315). Assuming a PSI monomer/-hydrogenase ratio of 1:1 and chlorophyll content of 100 Chl*a* per PS I molecule, our system generates up to 3.0 mmol H_2 h^{-1} per mg of chlorophyll, underlining the importance of improving electron transfer kinetics by coupling a hydrogenase to PS I as envisaged by Iwuchukwu *et al*.

Acknowledgment. We gratefully acknowledge financial support by the BMBF ($BioH_2$, Grundlagen für einen biotechnologischen und biomimetischen Ansatz der Wasserstoffproduktion), the EU/Energy Network project Solar-H2 (FP7 Contract No. 212508), and the DFG Cluster of Excellence "Unifying Concepts in Catalysis". We thank Prof. Dr. O. Kruse, A. Doebbe, Prof. Dr. N. Sewald, and K. Wollschläger (Bielefeld University) for introduction to and use of the 3000A Micro GC and the Biacore 3000 as well as for fruitful discussion. We are indebted to M. Kopczak and Prof. Dr. M. Rögner (Ruhr University Bochum) and U. Dühring and A. Wilde (Humboldt University of Berlin) for helpful instructions concerning cyanobacterial genetics and PS I purification.

Supporting Information Available: Kinetics of the assembly of the hybrid complex, surface enhancement factor, quantification of the hybrid complex, and midpoint potential of PMS. This material is available free of charge *via* the Internet at http://pubs.acs.org.

REFERENCES AND NOTES

1. Gray, H. B. Powering the Planet with Solar Fuel. *Nat. Chem.* **2009**, *1*, 7.
2. Jordan, P.; Fromme, P.; Witt, H. T.; Klukas, O.; Saenger, W.; Krauss, N. Three-Dimensional Structure of Cyanobacterial Photosystem I at 2.5 Å´ Resolution. *Nature* **2001**, *411*, 909–917.
3. Alivisatos, P.; Cummings, P.; Yoreo, J. D.; Fichthorn, K.; Gates, B.; Hwang, R.; Lowndes, D.; Majumdar, A.; Makowski, L.; Michalske, T. *Nanoscience Research for Energy Needs: Report of the National Nanotechnology Initiative*; The National Nanotechnology Coordination Office: Arlington, 2004.
4. Krabben, L.; Schlodder, E.; Jordan, R.; Carbonera, D.; Giacometti, G.; Lee, H.; Webber, A. N.; Lubitz, W. Influence of the Axial Ligands on the Spectral Properties of P700 of Photosystem I: A Study of Site-Directed Mutants. *Biochemistry* **2000**, *39*, 13012–13025.
5. Jordan, R.; Nessau, U.; Schlodder, E. Charge Recombination between the Iron−Sulphur Clusters and P700+. In *Photosynthesis: Mechanisms and Effects*, Garab, G., Ed.; Kluwer Academic Publishers: Dordrecht, The Netherlands, 1998; pp 663−666.
6. Das, R.; Kiley, P. J.; Segal, M.; Norville, J.; Yu, A. A.; Wang, L. Y.; Trammell, S. A.; Reddick, L. E.; Kumar, R.; Stellacci, F.; Lebedev, N.; Schnur, J.; Bruce, B. D.; Zhang, S. G.; Baldo, M. Integration of Photosynthetic Protein Molecular Complexes in Solid-State Electronic Devices. *Nano Lett.* **2004**, *4*, 1079–1083.
7. Carmeli, I.; Frolov, L.; Carmeli, C.; Richter, S. Photovoltaic Activity of Photosystem I-Based Self-Assembled Monolayer. *J. Am. Chem. Soc.* **2007**, *129*, 12352–12353.
8. Badura, A.; Esper, B.; Ataka, K.; Grunwald, C.; Wöll, C.; Kuhlmann, J.; Heberle, J.; Rögner, M. Light-Driven Water Splitting for (Bio-)Hydrogen Production: Photosystem 2 as the Central Part of a Bioelectrochemical Device. *Photochem. Photobiol.* **2006**, *82*, 1385–1390.
9. Terasaki, N.; Yamamoto, N.; Hiraga, T.; Sato, I.; Inoue, Y.; Yamada, S. Fabrication of Novel Photosystem I−Gold Nanoparticle Hybrids and their Photocurrent Enhancement. *Thin Solid Films* **2006**, *499*, 153–156.
10. Ciesielski, P. N.; Scott, A. M.; Faulkner, C. J.; Berron, B. J.; Cliffel, D. E.; Jennings, G. K. Functionalized Nanoporous Gold Leaf Electrode Films for the Immobilization of Photosystem I. *ACS Nano* **2008**, *2*, 2465–2472.
11. Grimme, R. A.; Lubner, C. E.; Bryant, D. A.; Golbeck, J. H. Photosystem I/Molecular Wire/Metal Nanoparticle Bioconjugates for the Photocatalytic Production of H_2. *J. Am. Chem. Soc.* **2008**, *130*, 6308–6309.
12. Vignais, P. M.; Billoud, B. Occurrence, Classification, and Biological Function of Hydrogenases: An Overview. *Chem. Rev.* **2007**, *107*, 4206–4272.
13. Armstrong, F. A.; Fontecilla-Camps, J. C. Biochemistry. A Natural Choice for Activating Hydrogen. *Science* **2008**, *321*, 498–499.
14. Vincent, K. A.; Parkin, A.; Lenz, O.; Albracht, S. P.; Fontecilla-Camps, J. C.; Cammack, R.; Friedrich, B.; Armstrong, F. A. Electrochemical Definitions of O_2 Sensitivity and Oxidative Inactivation in Hydrogenases. *J. Am. Chem. Soc.* **2005**, *127*, 18179–18189.
15. Baffert, C.; Demuez, M.; Cournac, L.; Burlat, B.; Guigliarelli, B.; Bertrand, P.; Girbal, L.; Leger, C. Hydrogen-Activating Enzymes: Activity Does Not Correlate with Oxygen Sensitivity. *Angew. Chem., Int. Ed.* **2008**, *47*, 2052–2054.
16. Goldet, G.; Wait, A. F.; Cracknell, J. A.; Vincent, K. A.; Ludwig, M.; Lenz, O.; Friedrich, B.; Armstrong, F. A. Hydrogen Production under Aerobic Conditions by Membrane-Bound Hydrogenases from *Ralstonia* Species. *J. Am. Chem. Soc.* **2008**, *130*, 11106–11113.
17. Krassen, H.; Stripp, S.; von, A. G.; Ataka, K.; Happe, T.; Heberle, J. Immobilization of the [FeFe]-Hydrogenase CrHydA1 on a Gold Electrode: Design of a Catalytic Surface for the Production of Molecular Hydrogen. *J. Biotechnol.* **2009**, *142*, 3–9.
18. Ghirardi, M. L.; Dubini, A.; Yu, J. P.; Maness, P. C. Photobiological Hydrogen-Producing Systems. *Chem. Soc. Rev.* **2009**, *38*, 52–61.
19. Hemschemeier, A.; Fouchard, S.; Cournac, L.; Peltier, G.; Happe, T. Hydrogen Production by *Chlamydomonas reinhardtii*: An Elaborate Interplay of Electron Sources and Sinks. *Planta* **2008**, *227*, 397–407.
20. Rupprecht, J.; Hankamer, B.; Mussgnug, J. H.; Ananyev, G.; Dismukes, C.; Kruse, O. Perspectives and Advances of Biological H_2 Production in Microorganisms. *Appl. Microbiol. Biotechnol.* **2006**, *72*, 442–449.
21. Melis, A.; Seibert, M.; Ghirardi, M. L. Hydrogen Fuel Production by Transgenic Microalgae. *Adv. Exp. Med. Biol.* **2007**, *616*, 108–121.
22. Ludwig, M.; Cracknell, J. A.; Vincent, K. A.; Armstrong, F. A.; Lenz, O. Oxygen-Tolerant H_2 Oxidation by Membrane-Bound [NiFe] Hydrogenases of *Ralstonia* Species. Coping with Low Level H_2 in Air. *J. Biol. Chem.* **2009**, *284*, 465–477.
23. Izawa, S.; Kraayenhof, R.; Ruuge, E. K.; DeVault, D. The Site of KCN Inhibition in the Photosynthetic Electron Transport Pathway. *Biochim. Biophys. Acta* **1973**, *314*, 328–339.

24. Ihara, M.; Nishihara, H.; Yoon, K. S.; Lenz, O.; Friedrich, B.; Nakamoto, H.; Kojima, K.; Honma, D.; Kamachi, T.; Okura, I. Light-Driven Hydrogen Production by a Hybrid Complex of a [NiFe]-Hydrogenase and the Cyanobacterial Photosystem I. *Photochem. Photobiol.* **2006**, *82*, 676–682.
25. Volbeda, A.; Garcin, E.; Piras, C.; deLacey, A. L.; Fernandez, V. M.; Hatchikian, E. C.; Frey, M.; Fontecilla-Camps, J. C. Structure of the [NiFe] Hydrogenase Active Site: Evidence for Biologically Uncommon Fe Ligands. *J. Am. Chem. Soc.* **1996**, *118*, 12989–12996.
26. Ataka, K.; Giess, F.; Knoll, W.; Naumann, R.; Haber-Pohlmeier, S.; Richter, B.; Heberle, J. Oriented Attachment and Membrane Reconstitution of His-Tagged Cytochrome *c* Oxidase to a Gold Electrode: *In Situ* Monitoring by Surface-Enhanced Infrared Absorption Spectroscopy. *J. Am. Chem. Soc.* **2004**, *126*, 16199–16206.
27. Fabian, H.; Mäntele, W. Infrared Spectroscopy of Proteins. In *Handbook of Vibrational Spectroscopy*, Chalmers, J. M., Griffiths, P. R., Eds.; Wiley: Chichester, U.K., 2002; pp 3399−3425.
28. Lushy, A.; Verchovsky, L.; Nechushtai, R. The Stable Assembly of Newly Synthesized PsaE into the Photosystem I Complex Occurring *via* the Exchange Mechanism is Facilitated by Electrostatic Interactions. *Biochemistry* **2002**, *41*, 11192–11199.
29. Cohen, Y.; Chitnis, V. P.; Nechushtai, R.; Chitnis, P. R. Stable Assembly of PsaE into Cyanobacterial Photosynthetic Membranes Is Dependent on the Presence of Other Accessory Subunits of Photosystem I. *Plant Mol. Biol.* **1993**, *23*, 895–900.
30. Armstrong, S. H.; Budka, M. J. E.; Morrison, K. C.; Hasson, M. Preparation and Properties of Serum and Plasma Proteins 0.12. The Refractive Properties of the Proteins of Human Plasma and Certain Purified Fractions. *J. Am. Chem. Soc.* **1947**, *69*, 1747–1753.
31. Stenberg, E.; Persson, B.; Roos, H.; Urbaniczky, C. Quantitative-Determination of Surface Concentration of Protein with Surface-Plasmon Resonance Using Radiolabeled Proteins. *J. Colloid Interface Sci.* **1991**, *143*, 513–526.
32. Jeanjean, R.; Latifi, A.; Matthijs, H. C.; Havaux, M. The PsaE Subunit of Photosystem I Prevents Light-Induced Formation of Reduced Oxygen Species in the Cyanobacterium *Synechocystis* sp. PCC 6803. *Biochim. Biophys. Acta* **2008**, *1777*, 308–316.
33. Gobets, B.; van, G. R. Energy Transfer and Trapping in Photosystem I. *Biochim. Biophys. Acta* **2001**, *1507*, 80–99.
34. Evans, M. C.; Heathcote, P. Effects of Glycerol on the Redox Properties of the Electron Acceptor Complex in Spinach Photosystem I Particles. *Biochim. Biophys. Acta* **1980**, *590*, 89–96.
35. Uchida, T.; Mogami, H.; Yamakata, A.; Sasaki, Y.; Osawa, M. Hydrogen Evolution Reaction Catalyzed by Proton-Coupled Redox Cycle of 4,4′-Bipyridine Monolayer Adsorbed on Silver Electrodes. *J. Am. Chem. Soc.* **2008**, *130*, 10862–10863.
36. Tamamushi, R.; Tanaka, K. Effect of Methylviologen on the Hydrogen Evolution at Mercury-Electrodes in Aqueous Buffer Solutions. *J. Electroanal. Chem.* **1987**, *230*, 177–188.
37. Hamelin, A.; Morin, S.; Richer, J.; Lipkowski, J. Adsorption of Pyridine on the (311) Face of Silver. *J. Electroanal. Chem.* **1990**, *285*, 249–262.
38. Hamelin, A.; Morin, S.; Richer, J.; Lipkowski, J. Adsorption of Pyridine on the (210) Face of Silver. *J. Electroanal. Chem.* **1991**, *304*, 195–209.
39. Wisitruangsakul, N.; Lenz, O.; Ludwig, M.; Friedrich, B.; Lendzian, F.; Hildebrandt, P.; Zebger, I. Monitoring Catalysis of the Membrane-Bound Hydrogenase from *Ralstonia eutropha* H16 by Surface-Enhanced IR Absorption Spectroscopy. *Angew. Chem., Int. Ed.* **2009**, *48*, 611–613.
40. Ataka, K.; Heberle, J. Biochemical Applications of Surface-Enhanced Infrared Absorption Spectroscopy. *Anal. Bioanal. Chem* **2007**, *388*, 47–54.
41. Ataka, K.; Heberle, J. Electrochemically Induced Surface-Enhanced Infrared Difference Absorption (SEIDA) Spectroscopy of a Protein Monolayer. *J. Am. Chem. Soc.* **2003**, *125*, 4986–4987.
42. Miyake, H.; Ye, S.; Osawa, M. Electroless Deposition of Gold Thin Films on Silicon for Surface-Enhanced Infrared Spectroelectrochemistry. *Electrochem. Commun.* **2002**, *4*, 973–977.